Electron-proton relaxation in hot-dense plasmas with a screened quantum statistical potential

Zhengfeng Fan,[1,2,*] Chengxin Yu,[1,*] Cong-Zhang Gao,[1,†] Xuefeng Xu,[1] Cunbo Zhang,[1] Binbing Wu,[1] Jie Liu,[3,2] Pei Wang,[1,2,‡] and Shaoping Zhu[1,2]

[1]*Institute of Applied Physics and Computational Mathematics, Beijing 100088, China*

[2]*HEDPS, Center for Applied Physics and Technology, and College of Engineering, Peking University, Beijing 100871, China*

[3]*Graduate School of China Academy of Engineering Physics, Beijing 100193, China*

(Received 28 January 2024; accepted 17 July 2024; published 6 August 2024)

Modeling the nonequilibrium process between ions and electrons is of great importance in laboratory fusion ignition, laser-plasma interaction, and astrophysics. For hot and dense plasmas, theoretical descriptions of Coulomb collisions remain complicated due to quantum effect at short distances and screening effect at long distances. In this paper, we propose an analytical screened quantum statistical potential that takes into account both the short-range quantum diffraction effect and the long-range screening effect. By implementing the newly developed potential into the binary scattering framework, the electron-proton temperature relaxation in hot-dense hydrogen plasmas is investigated. In both the classical and quantum limits, analytical expressions for the Coulomb logarithm have been obtained, which are generally embedded in an asymptotic matching formula. Quantitative comparisons with molecular dynamics simulations and recent OMEGA experiments demonstrate that the present modeling is well suited to describe the temperature relaxation process between electrons and ions in hot-dense plasmas.

DOI: 10.1103/PhysRevE.110.025202

I. INTRODUCTION

Nonequilibrium between electrons and ions is an important phenomenon that occurs in extreme and transient conditions, such as laboratory fusion ignition [1–8], laser-driven plasmas [9–11], ultracold plasmas [12–14], and astrophysics [15,16]. Accurate modeling of the nonequilibrium process requires reliable relaxation models between electrons and ions.

Pioneering works on the temperature relaxation between electrons and ions in weakly coupled plasmas were accomplished by Landau [17] and Spitzer [18] (LS), and the electron-ion temperature relaxation time can be analytically expressed as

$$\tau_{\mathrm{ei}} = \frac{3m_{\mathrm{e}}m_{\mathrm{i}}}{8\sqrt{2\pi}Z^2e^4n_{\mathrm{i}}}\left(\frac{k_{\mathrm{B}}T_{\mathrm{e}}}{m_{\mathrm{e}}}+\frac{k_{\mathrm{B}}T_{\mathrm{i}}}{m_{\mathrm{i}}}\right)^{3/2}\frac{1}{\ln\Lambda}, \tag{1}$$

where n_{i} is the number density of ions, $m_{\mathrm{e}}(m_{\mathrm{i}})$ is the electron (ion) mass, $T_{\mathrm{e}}(T_{\mathrm{i}})$ is the electron (ion) temperature, e and Z are the electron charge and ion charge states, respectively, and k_{B} is the Boltzmann constant. Applying this expression to specified plasmas conditions, the accuracy of the electron-ion relaxation time relies uniquely on the so-called Coulomb logarithm $\ln\Lambda$, which principally accounts for complex effects of charged particles' collision physics in plasmas. Usually, it is simplified as $\ln\Lambda = \ln(b_{\max}/b_{\min})$, where $b_{\max}$ and $b_{\min}$ are truncating limits in the integral of the form $\int \mathrm{d}b/b$; otherwise, the integral would be divergent [19]. The divergence as $b\to\infty$ is caused by the absence of a long-range many-body screening effect, and $b_{\max}$ is typically truncated at the electron Debye screening length $\lambda_{\mathrm{D}} = \sqrt{k_{\mathrm{B}}T_{\mathrm{e}}/4\pi e^2 n_{\mathrm{e}}}$. The divergence as $b\to 0$ is caused by a weak-scattering assumption, and $b_{\min}$ is usually assigned as the maximum of the Landau length $\lambda_{\mathrm{L}} = Ze^2/k_{\mathrm{B}}T_{\mathrm{e}}$ and the electron thermal de Broglie wavelength $\lambda_{\mathrm{th}} = \hbar\sqrt{2\pi/m_{\mathrm{e}}k_{\mathrm{B}}T_{\mathrm{e}}}$, where $\hbar$ is the reduced Planck constant.

Theories have been developed to deal with the long-range screening and short-range quantum effects [20–33], so as to obtain more self-consistent expressions of $\ln\Lambda$. Typically, Brown, Preston, and Singleton (BPS) utilized dimensional continuation to obtain a new result accurate to second order in the plasma coupling parameter [28,29]. For nondegenerate plasmas, their result can be written as

$$\begin{aligned}\ln\Lambda_{\mathrm{BPS}} &= \ln\Lambda^{\mathrm{QM}} + \ln\Lambda^{\Delta\mathrm{C}},\\ \ln\Lambda^{\mathrm{QM}} &= \ln\frac{4\sqrt{\pi}\lambda_{\mathrm{D}}}{\lambda_{\mathrm{th}}} - \frac{\gamma+1}{2},\\ \ln\Lambda^{\Delta\mathrm{C}} &= -\frac{e_{\mathrm{H}}}{k_{\mathrm{B}}T_{\mathrm{e}}}Z^2\left[\zeta_3\left(\ln\frac{k_{\mathrm{B}}T_{\mathrm{e}}}{Z^2e_{\mathrm{H}}}-\gamma\right)-2\zeta_3'\right],\end{aligned} \tag{2}$$

where $\ln\Lambda^{\mathrm{QM}}$ incorporates quantum diffraction effect, $\ln\Lambda^{\Delta\mathrm{C}}$ is a classical correction when the plasma parameters depart from the extreme quantum limit, γ is the Euler constant, e_{H} is the binding energy of the hydrogen atom, $\zeta_3 = 1.20205$, and $\zeta_3' = -0.19812$. On the other hand, Gericke, Murillo, and Schlanges (GMS) developed a T-matrix theory to verify various approximations of $\ln\Lambda$, and they ultimately suggested

*These authors contributed equally to this work.
†Contact author: gao_congzhang@iapcm.ac.cn
‡Contact author: wangpei@iapcm.ac.cn

an effective Coulomb logarithm [27]

$$\ln \Lambda_{\rm GMS} = \frac{1}{2}\ln\left(1+\frac{\lambda_{\rm D}^2+R_{\rm i}^2}{\lambda_{\rm th}^2/8\pi+\lambda_{\rm L}^2}\right), \tag{3}$$

where $R_{\rm i} = (3/4\pi n_{\rm i})$ is the ion sphere radius.

In the classical and weak-coupling limit, i.e., $\lambda_{\rm th} \to 0$ and $\lambda_{\rm L} \ll \lambda_{\rm D}$, theories of Kihara and Aono (KA) [23], BPS [29], and Baalrud and Daligault (BD) [30] all converge to a same result of $\ln\Lambda \to \ln({\rm C}/g_e)$ with $g_e = \lambda_{\rm L}/\lambda_{\rm D}$ and ${\rm C} = 0.77$, and this result has been confirmed through molecular dynamics simulations by Dimonte and Daligault [34]. However, for hot-dense plasmas such as the fusion-burning regime in inertial confinement fusion, $\lambda_{\rm th}$ becomes much larger than $\lambda_{\rm L}$, then quantum effect would dominate in short-range collisions. In the quantum limit, if we write $\ln\Lambda$ as $\ln({\rm D}/h_e)$ where $h_e = \lambda_{\rm th}/\lambda_{\rm D}$, then ${\rm D}_{\rm BPS} = 3.22$ while ${\rm D}_{\rm GMS} = 5.01$. The difference between BPS and GMS is apparent, indicating that there exists inconsistency in our understanding of the quantum effect in electron-ion relaxation. As the electron-ion relaxation in plasmas mostly concerns the energy transfer between two species, the application of binary scattering method has a long history in this field, but it requires a vigorous effort to adequately and accurately address both the short-range quantum effect and the long-range screening effect. In this study, we propose a screened quantum statistical potential (SQSP) that is applied in the binary scattering method to study the electron-proton temperature relaxation in hot-dense hydrogen plasmas. Results have been obtained, and comparisons with molecular dynamics simulations and existing experiments demonstrate the accuracy of the present modeling.

This paper is organized as follows. Section II introduces the SQSP. Section III presents our results for electron-proton relaxation and its validations. Finally, a brief summary is given in Sec. IV.

II. SCREENED QUANTUM STATISTICAL POTENTIAL

The binary scattering method treats electrons and ions as classical particles and thus requires an effective potential to account for both the quantum and screening effects. Even though there are numerous effective approaches that address these two effects separately or jointly, we still lack a solution that properly addresses both of these two effects. First, for the quantum effect, several quantum statistical potentials (QSPs) have been proposed and are widely used in molecular dynamics (MD) simulations [35–39]. Following the derivations in Ref. [40], the QSP for a pair of particles could be defined as

$$U(r) = -\frac{1}{\beta}\ln\left[\frac{\rho_2(\mathbf{r},\mathbf{r},\beta)}{\rho_{\rm F}(\mathbf{r},\mathbf{r},\beta)}\right], \tag{4}$$

where $\rho_2(\mathbf{r},\mathbf{r},\beta)$ is the pair density matrix, $\rho_{\rm F}(\mathbf{r},\mathbf{r},\beta)$ is the free particle density matrix, $\beta = 1/k_{\rm B}T$, and $r = |\mathbf{r}|$. The Dunn-Broyles (DB) potential [41], also known as the Hansen-McDonald potential [42], adds a diffractive correction to the Coulomb potential and is represented as

$$U_{\rm ab}(r) = \frac{q_{\rm a}q_{\rm b}}{r}(1-\mathbf{e}^{-2\pi\hat{r}}), \tag{5}$$

where $\hat{r} = r/\lambda_{\rm ab}$, and $\lambda_{\rm ab}$ is the thermal de Broglie wavelength with respect to the reduced mass of particles a and b.

TABLE I. Fitting parameters for e-p and e-e interactions in the improved DB potential.

	c_0	c_1	c_2	c_3	c_4	c_5
e-p	0.1637	25.72	−1.111	9.500	0.7389	12.86
e-e	0.07418	12.76	0.6461	9.066	0.6190	14.64

Simple as it is, the DB potential has a maximum error of more than 10% when compared with the results calculated from Eq. (4). The Kelbg or modified-Kelbg formula provides better accuracy; however, its parameters are usually temperature dependent [36,40]. In the present study, we propose an improved DB potential as

$$U_{\rm ab}^{\rm I}(r) = \frac{q_{\rm a}q_{\rm b}}{r}[1-\mathbf{e}^{-(2\pi+c_0\hat{\lambda}_{\rm ab})\hat{r}}+\eta(\hat{r})], \tag{6}$$

where

$$\eta(\hat{r}) = \left(c_1+\frac{c_2}{\hat{\lambda}_{\rm ab}}\right)(\mathbf{e}^{-c_3\hat{r}}-c_4\mathbf{e}^{-c_5\hat{r}})\hat{r}^2, \tag{7}$$

where c_i (with i ranging from one to five) are dimensionless and temperature-independent parameters, and $\hat{\lambda}_{\rm ab} = \lambda_{\rm ab}/{\rm a}_0$ with $\rm a_0$ being the Bohr radius. The improvement associated with c_0 is used to recover the correct asymptotic behavior at $r = 0$, and the term $\eta(\hat{r})$ is added to retrieve the physical profile of the distance-dependent potential. With these improvements, the maximum error of the improved DB potential is satisfactorily controlled within 1% when compared with the results of Eq. (4). For e-e pair interactions, it is recommended to add the Pauli exclusion term, as suggested by Deutsch [43], to Eq. (6). Table I lists the fitting parameters for electron-proton (e-p) and electron-electron (e-e) pair interactions.

Another benefit of the improved DB potential is that it enables us to obtain an analytical SQSP. Substituting $U_{\rm ep}^{\rm I}(r)/e$ into the Poisson equation and noticing that $m_{\rm e} \ll m_{\rm i}$, the electron charge density distribution function is derived as

$$n_{\rm e}(r) = -\frac{e}{4\pi\lambda_{th}^3}\left\{\frac{c_6^2\mathbf{e}^{-c_6\hat{r}}}{\hat{r}}+c_7[\varsigma(c_3,\hat{r})-c_4\varsigma(c_5,\hat{r})]\right\}, \tag{8}$$

where

$$\varsigma(\alpha,\hat{r}) = -\frac{\mathbf{e}^{-\alpha\hat{r}}}{\hat{r}}(\alpha^2\hat{r}^2-4\alpha\hat{r}+2), \tag{9}$$

$c_6 = (2\pi+c_0\hat{\lambda}_{th})$, and $c_7 = c_1+c_2/\hat{\lambda}_{\rm th}$. Protons are still treated as point charges, and its screened potential is assumed to be classical, i.e.,

$$\phi^{\rm S}(r) = e/r\cdot\exp(-r/\lambda_{\rm D}), \tag{10}$$

then the SQSP for an e-p pair is derived as

$$\begin{aligned} U_{\rm ep}^{\rm I\text{-}S}(r) &= \int\phi^{\rm S}(|\mathbf{r}-\mathbf{r}'|)n_{\rm e}(\mathbf{r}')\mathrm{d}^3\mathbf{r}' \\ &= -\frac{e^2}{r}\{\Phi(\hat{r},\tilde{r})+c_7[\Psi(c_3,\hat{r},\tilde{r})-c_4\Psi(c_5,\hat{r},\tilde{r})]\}, \end{aligned} \tag{11}$$

where

$$\Phi(\hat{r},\tilde{r}) = \frac{\mathbf{e}^{-\tilde{r}} - \mathbf{e}^{-c_6\hat{r}}}{1-(\tilde{\lambda}_{\rm th}/c_6)^2}, \tag{12}$$

$$\Psi(\alpha,\hat{r},\tilde{r}) = \frac{\Xi_2\mathbf{e}^{-\tilde{r}} + (-\Xi_2+\Xi_3\tilde{r}+\Xi_4\tilde{r}^2)\mathbf{e}^{-\alpha\hat{r}}}{\Xi_1}, \tag{13}$$

$$\Xi_1 = \tilde{\lambda}_{\rm th}^2(\alpha-\tilde{\lambda}_{\rm th})^3(\alpha+\tilde{\lambda}_{\rm th})^3, \tag{14}$$

$$\Xi_2 = -2\tilde{\lambda}_{\rm th}^4\left(3\alpha^2+\tilde{\lambda}_{\rm th}^2\right), \tag{15}$$

$$\Xi_3 = 4\alpha\tilde{\lambda}_{\rm th}^3\left(\alpha^2-\tilde{\lambda}_{\rm th}^2\right), \tag{16}$$

$$\Xi_4 = \alpha^2\left(\alpha^2-\tilde{\lambda}_{\rm th}^2\right)^2, \tag{17}$$

$\tilde{r} = r/\lambda_{\rm D}$, and $\tilde{\lambda}_{\rm th} = \lambda_{\rm th}/\lambda_{\rm D}$.

It is worth noting that the SQSP satisfies the following two limits: First, as $\tilde{r}\to 0$, the screening effect is negligible and it approaches the pair interaction limit that $U_{\rm ep}^{\rm I\text{-}S}(r)\to U_{\rm ep}^{\rm I}(r)$; Second, as $\lambda_{\rm th}\to 0$, it approaches the classical screened potential limit that $U_{\rm ep}^{\rm I\text{-}S}(r)\to -e\cdot\phi^{\rm S}(r)$. For more general situations, we utilize the effective potential theory (EPT) developed in Ref. [30] to validate the SQSP. The effective potential is related to the pair distribution function $g(r)$ as $U_{\rm ep}^{\rm EPT}(r) = -k_BT\ln[g(r)]$. The pair distribution function $g(r)$ is numerically solved using the coupled Ornstein-Zernike relation and the hypernetted chain closure [44].

In the present study, electrons are treated as negative-charged particles rather than positrons as used in Ref. [30]. For bare Coulomb potential ($U_{ep}\sim 1/r$), the energy exchange rate is symmetric with respect to the charge sign of the participating particles. However, the charge-sign symmetry breaks down when the particles collide at a distance comparable to or shorter than the electronic thermal de Broglie wavelength, which is often referred to as the "Barkas effect" [45,46]. It has been stated in Ref. [28] that the "Barkas effect" is of order $O(g_e^3)$ and is often neglected [34]. For plasmas temperature at ~keV, it is most probably important and cannot be simply discarded. Within the SQSP model, the "Barkas effect" is intrinsically incorporated, such that we could achieve better accuracy than neglecting it.

Figure 1 shows a comparison of the normalized e-p pair potential obtained from the SQSP and the EPT for three different mass densities at $T = 100$ eV. Corresponding results of the (density-independent) improved DB potential and the classical screened potential are also presented. For $\rho = 0.1$ g/cm^3 and 1.5 g/cm^3, the SQSP results agree excellently with those of the EPT. As the density increases to 30 g/cm^3 where $g_e = 0.82$, the accuracy of the SQSP begins to decrease due to strong coupling effect. It is clear that the analytical SQSP preserves the asymptotics at both the short and long distances; in contrast, the improved DB potential overestimates it at longer distances due to the absence of the screening effect, and the classical screened potential without the quantum diffraction effect overestimates it at shorter distances. For the SQSP, there approximately exists a valid region by setting $\max_r[|U_{\rm ep}^{\rm I\text{-}S}(r) - U_{\rm ep}^{\rm EPT}(r)|/U_{\rm ep}^{\rm EPT}(r)] < 5\%$, in which the plasmas condition must fulfill the relationship of $T > 25.6\rho^{0.71}$ and $g_e < 0.9$, with T and ρ in units of eV and g/cm^3, respectively.

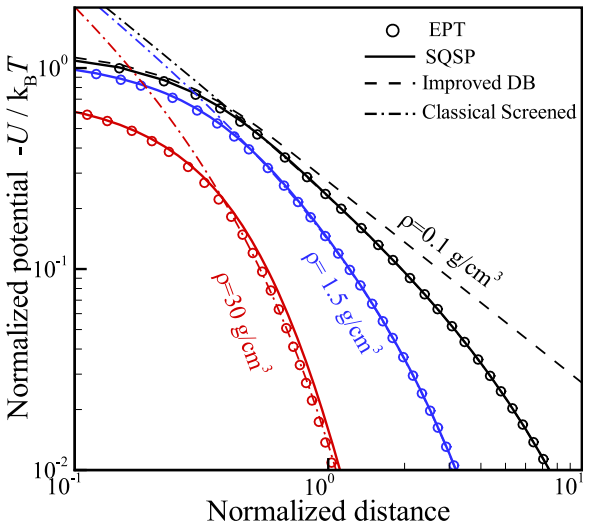

FIG. 1. Normalized e-p pair potential obtained from the SQSP (solid lines), the EPT of Ref. [30] (circles), the improved DB potential (dashed line), and the classical screened potential (dash dot lines) for $T = 100$ eV and $\rho = 0.1$ g/cm^3, 1.5 g/cm^3 and 30 g/cm^3, respectively. The horizontal axis is normalized by the Bohr radius a_0.

III. RESULTS FOR ELECTRON-PROTON RELAXATION

A. Formulas for the Coulomb logarithm

Knowing the SQSP, it is straightforward to obtain the e-p energy transfer rate following a routine procedure. First, the scattering angle of a binary e-p collision in the center-of-mass framework is written as

$$\theta = \pi - 2b\int_{r_{\rm min}}^{\infty}\frac{{\rm d}r}{r^2}\Big/\sqrt{1-\frac{b^2}{r^2}-\frac{U_{\rm ep}^{\rm I\text{-}S}(r)}{E_{\rm ep}}}, \tag{18}$$

where v, b, and $r_{\rm min}$ denote the e-p scalar relative velocity, the impact parameter, and the minimum distance of collision, respectively. The kinetic energy is defined as $E_{\rm ep} = \mu v^2/2$ with the reduced mass $\mu = m_{\rm p}m_{\rm e}/(m_{\rm p}+m_{\rm p})$. Second, the energy transfer cross section is given by

$$\sigma = 2\pi\int_0^{\infty}[1-\cos(\theta)]b{\rm d}b. \tag{19}$$

Finally, the energy transfer rate between the electrons and protons of two-temperature plasmas is obtained as

$$\frac{{\rm d}\left(\frac{3}{2}k_{\rm B}T_{\rm e}\right)}{{\rm d}t} = -\frac{3k_{\rm B}(T_{\rm e}-T_{\rm i})}{2\tau_{\rm ei}} = -mn_{\rm p}\iint(\mathbf{V}\cdot\mathbf{v})v\sigma f(\mathbf{v}_e)f(\mathbf{v}_p)d\mathbf{v}_e d\mathbf{v}_p, \tag{20}$$

where $\mathbf{V}$ and $\mathbf{v}$ are the center-of-mass velocity and relative velocity of an e-p pair, and f represents the Maxwellian velocity distribution of electrons or protons.

The e-p relaxation time or Coulomb logarithm is ready to be obtained by solving the combined Eqs. of (1), (11), and (18)–(20) numerically. When $\lambda_{\rm th}\ll\lambda_{\rm L}$ or $h_e\ll g_e$, it approaches the classical limit where $\ln\Lambda$ depends solely on g_e. In practice, numerical calculations for the classical limit have been carried out by using the classical screened potential, i.e., $U_{\rm ep}^{\rm I\text{-}S}(r) = -e\cdot\phi^{\rm S}(r)$. In order to obtain an analytical

expression of the Coulomb logarithm, numerical results for $g_e < 0.9$ have been fitted as

$$\ln \Lambda^{\mathrm{C}} = \ln\left[1 + \frac{0.77}{\min\left(g_{\mathrm{e}}, 0.55 g_{\mathrm{e}}^{0.88}\right)}\right], \tag{21}$$

where the relative error is lower than 2.3%. It is to be noted that Eq. (21) is reduced to $\ln(1 + 0.77/g_{\mathrm{e}})$ in the weak-coupling limit, which coincides with the well-established results by KA [23], BPS [29], BD [30] *et al.* Likewise, when $\lambda_{\mathrm{th}} \gg \lambda_{\mathrm{L}}$ or $h_e \gg g_e$, it approaches the quantum limit where $\ln \Lambda$ only depends on h_e. To make it tractable, the quantum limit is approximated by setting $\lambda_{\mathrm{L}} = 2\%\lambda_{\mathrm{th}}$, or equivalently $T_e = 10$ keV, and evaluations with decreasing λ_{L} suggest that the approximation error is much less than 1%. In the quantum limit, $\ln \Lambda$ for $h_e < 2.0$ is fitted as

$$\ln \Lambda^{\mathrm{Q}} = \ln\left(0.52 + \frac{2.39}{h_{\mathrm{e}}}\right), \tag{22}$$

and the error relative to the numerical data is less than 1.5%. The quantum limit of the present result is slightly lower than that of BPS and GMS.

For a general case, an asymptotic matching formula is generalized as

$$\ln \Lambda = [(\ln \Lambda^{\mathrm{C}})^{-p} + (\ln \Lambda^{\mathrm{Q}})^{-p}]^{-1/p}, \tag{23}$$

where the parameter p depends on g_e and h_e, and is parametrized as

$$p(g_{\mathrm{e}}, h_{\mathrm{e}}) = 0.61 - 1.14 \ln(g_{\mathrm{e}}) + 0.45 \ln(h_{\mathrm{e}}). \tag{24}$$

The relative error of Eq. (23) is less than 2.5% for $T > \max(25.6\rho^{0.71}, 121\rho^{0.45})$, where T and ρ are in units of eV and g/cm^3, respectively. In the valid region where the maximum relative error between our SQSP and the EPT of Ref. [30] is less than 5%, p is supposed to be larger than 0.8. Then, a combination of Eqs. (1) and (21)–(24) represents the result of the present modeling of e-p temperature relaxation for hot-dense hydrogen plasmas.

B. Comparison with MD simulations

In this subsection, we compare our new model and the widely used theories of LS, GMS, and BPS with MD simulations. The MD simulations are performed by our parallel code, FlexibleMD, using the improved DB potential as described in Eq. (5) along with a Pauli exclusion term as suggested by Deutsch [43]. The improved DB potential, as well as the Pauli exclusion term, changes instantaneously with the electron temperature which is updated every 100 time steps. These simulations adopt the Velocity-Verlet algorithm [48] and utilize periodic boundary conditions. By varying the system size (i.e., the total number of electrons and protons) in a wide range from 10^4 to 10^6, it is fixed at 13 824 since the statistical noise of simulated temperature relaxation is already negligible in this case, see the Appendix. The time step is strictly controlled to conserve total energy ($\Delta E/E < 0.15\%$). Mass scaling treatment using a proton-to-electron ratio of ∼90 is employed to accelerate MD simulations, and MD-simulated e-p relaxation times should be rescaled to the real mass ratio of protons to electrons. Besides, a correct initial state of MD simulations is a prerequisite for electron-proton temperature relaxation, thus, a description of preparing the initial state of a two-temperature plasma and its numerical examination is provided in the Appendix.

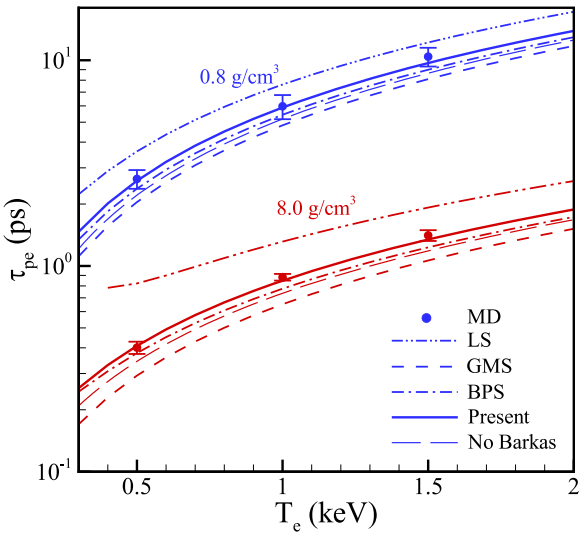

FIG. 2. Comparison of theoretical results (dash dot dot line for the LS model, dash dot line for the GMS model, dash line for the BPS model, solid line for the present model, and long dash line for the result without "Barkas effect") and MD simulations (dots with error bars) of e-p relaxation time for $\rho = 0.8$ g/cm^3 and 8.0 g/cm^3.

The e-p relaxation time τ_{ep} for a single MD simulation is extracted by using a partial relaxation approach [39], in which the temperature difference ($\Delta T = T_e - T_i$) is fitted to an exponential formula $\Delta T_0 \exp(-2t/\tau_{ep})$ during a short period with ΔT_0 being the initial temperature difference and τ_{ep} being the fitting parameter. In our recent study [39], we have demonstrated that the partial relaxation approach is reliable. In a short period, the electron temperature change is as little as ∼1%, so that τ_{ep} is associated with the initial electron temperature. The e-p relaxation time is finally determined by taking the ensemble average over 4–6 simulation samples, and the standard deviation (1σ) is used to represent the statistical uncertainty. Figure 2 compares our new results [Eq. (23), solid line] and widely used theories of LS (dash dot dot lines), GMS (dash dot lines), and BPS (dashed lines) with MD simulations (dots with error bars) for $\rho = 0.8$ g/cm^3 and 8.0 g/cm^3. For a quantitative comparison, the results for density and temperature states considered are listed in Table II. It is shown that the LS results lead to the largest errors; the GMS results have relative errors ranging from 19% to 27%; the BPS results reduce the relative errors to 9%–14%. It is seen that the BPS theory is more predictable than the LS and GMS models, however, BPS results are not always within the error bars of MD simulations for hot-dense plasma conditions considered here; and the present model exhibits the highest level of accuracy, with all results falling within the error bars of the MD simulations, see Table II. To be intuitive, we also show in Fig. 2 and Table II our corresponding results using like charges where the "Barkas effect" is excluded. It is found that the BPS results resemble our results without "Barkas effect."

TABLE II. For e-p relaxation time, quantitative comparison of theoretical results and MD simulations. The relaxation time is in units of picoseconds (ps). Bold styles mark the results that are beyond the uncertainty of MD simulations.

ρ (g/cm^3)	T_e (keV)	MD	LS	GMS	BPS	Present	No Barkas
0.8	0.5	2.649 ± 0.277	**3.606**	**2.044**	2.377	2.595	**2.208**
0.8	1.0	5.972 ± 0.803	**7.622**	**4.828**	5.435	5.891	5.178
0.8	1.5	10.41 ± 1.087	**12.20**	**8.097**	**8.995**	9.691	**8.647**
8.0	0.5	0.401 ± 0.028	**0.823**	**0.293**	0.377	0.409	**0.344**
8.0	1.0	0.882 ± 0.033	**1.313**	**0.652**	**0.776**	0.849	**0.737**
8.0	1.5	1.408 ± 0.084	**1.923**	**1.063**	**1.231**	1.344	**1.184**

Therefore, the inclusion of the "Barkas effect" in the present model enables us to obtain better results than the BPS model.

C. Comparison with recent experiments

In this subsection, we do comparisons with OMEGA experiments on the the ion-electron energy-transfer cross section in the high-energy-density regime [49]. In these experiments, shock-driven implosions of capsules filled with D^3He gas doped with a trace amount of argon are used to generate hot-dense hot-spot conditions, and the energy loss of 1 MeV DD tritons and 3.7 MeV D^3He alphas that have velocities lower than the average velocity of the thermal electrons is measured, and is used to determine the ion-electron energy-transfer cross section. Hot-spot conditions in these experiments approach the quantum limit, and the Coulomb logarithm should depend only on the electron density and electron temperature. Therefore, these experiments are suitable for validating the present model in the quantum limit.

Table III lists the experimental results and the theoretical results computed from the quantum limits of LS, GMS, BPS, and the present model. The Coulomb logarithms of the LS model are the smallest among the four theoretical models, and almost half of them fall outside the range of experimental uncertainties. The present model results are approximately 0.7–0.8 smaller than the GMS model and about 0.3 smaller than the BPS model. The GMS model tends to overestimate the Coulomb logarithm, due to the fact that its Coulomb logarithm of shot 78 608 has exceeded the upper limit of the experimental uncertainty. Nevertheless, the uncertainties of these OMEGA experimental results are ranging from 24% (shot 75 694) to 32% (shot 78 609) which is too appreciable to distinguish the BPS theory and the present model, and more accurate measurements are required to demonstrate our improvements experimentally.

TABLE III. Comparison of theoretical results (LS, GMS, BPS, and the present one) and experimental results of Ref. [49]. Bold styles mark the results that are beyond the uncertainty of the experiments.

	n_e	T_e	ln Λ				
Shot	($\times 10^{23}$cm^{-3})	(keV)	Exp	Present	LS	GMS	BPS
78608	21 ± 4.2	1.4 ± 0.1	2.9 ± 0.8	3.2	2.3	**4.0**	3.5
78609	21 ± 4.2	1.4 ± 0.1	3.4 ± 1.1	3.2	2.3	4.0	3.5
78611	11 ± 4.5	1.6 ± 0.2	4.1 ± 1.1	3.7	**2.8**	4.4	4.0
78612	11 ± 4.5	1.6 ± 0.2	4.0 ± 1.1	3.7	**2.8**	4.4	4.0
75694	6.6 ± 1.0	2.8 ± 0.3	5.8 ± 1.4	4.5	**3.6**	5.2	4.8
75695	4.6 ± 0.7	2.3 ± 0.2	5.1 ± 1.5	4.5	3.6	5.2	4.8
75698	4.8 ± 0.7	2.1 ± 0.2	5.3 ± 1.4	4.4	**3.5**	5.1	4.7
75699	3.9 ± 0.6	1.9 ± 0.2	5.4 ± 1.5	4.4	**3.5**	5.1	4.7
75700	3.8 ± 0.6	1.9 ± 0.2	4.4 ± 1.2	4.4	3.5	5.1	4.7
75701	5.1 ± 0.8	1.8 ± 0.2	4.2 ± 1.2	4.2	3.3	4.9	4.5
75702	3.8 ± 0.8	1.4 ± 0.2	3.9 ± 1.1	4.1	3.2	4.8	4.4

IV. SUMMARY

In conclusion, an analytical screened quantum statistical potential is derived and applied in the binary scattering method to model the temperature relaxation between electrons and protons in hot and dense hydrogen plasmas. This potential provides a satisfactory description of both the short-range quantum effect and the long-range screening effect. Comparisons with molecular dynamics simulations and existing experiments demonstrate the accuracy of the present modeling. The present model has limitations for strongly coupled plasmas or relativistic cases, which also exists in other well-known models and will be addressed in the near future.

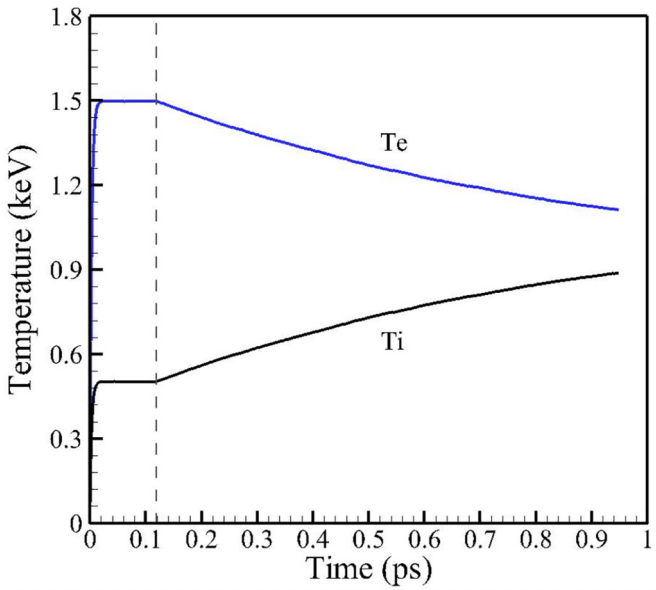

FIG. 3. Temperature relaxation within 1 ps for the plasma condition of $\rho = 8.0$ g/cm^3 and $T_e = 1.5$ keV.

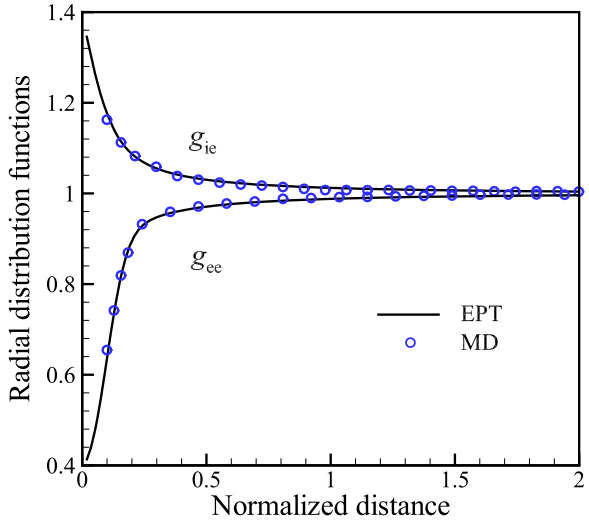

FIG. 4. Initial radial distributions. Solid curves are results obtained by the EPT method [30]. Plasma condition is the same as Fig. 3.

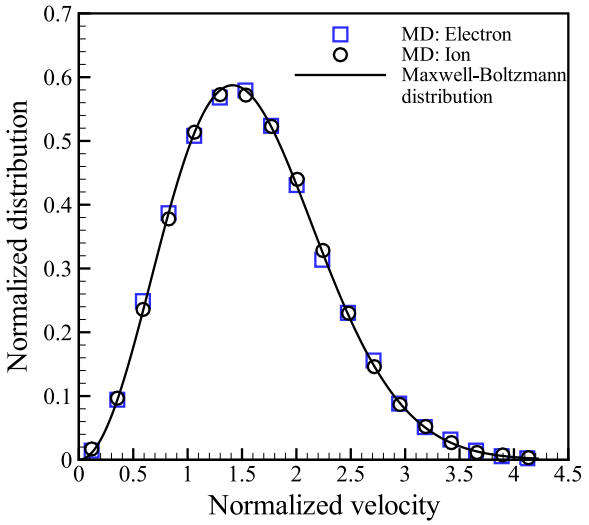

FIG. 5. Initial velocity distributions. Solid curves are analytical MB function. To compare the electrons and ions on the same scale, it is normalized by $\sqrt{kT/m}$ where m is electron or proton mass. Plasma condition is the same as Fig. 3.

ACKNOWLEDGMENT

This work has been supported by the National Natural Science Foundation of China (Grants No. 12375235 and No. 11975054).

APPENDIX: THE INITIAL STATE OF MD SIMULATIONS

An initial plasma state with separate electron and proton temperatures is well prepared in MD simulations following two main steps. First, the electrons and protons are generated with random positions in the selected simulation domain, and initial particle velocities are randomly sampled from the Maxwell-Boltzmann distribution at room temperature. Second, two thermostats [47] are separately applied for electrons and protons, in order to heat them up to different temperatures. A sufficient time interval is maintained to ensure that the particles of the same kind are fully relaxed, i.e., the electrons/protons follow Maxwell-Boltzmann (MB) distributions in the velocity space and satisfy correct initial radial distributions in the spatial space.

As an illustration, Figs. 3–5 present the electron-proton temperature relaxation within 1 ps, initial radial distribution, and particle's velocity distribution, respectively, for one of the MD simulations with plasma condition of $\rho = 8.0$ g/cm^3, $T_e = 1.5$ keV, and $T_i = 0.5$ keV. As can be seen, MD-simulated initial two-temperature plasma states should be correct, since both initial particles' radial distributions (Fig. 4) and velocity distributions (Fig. 5) agree satisfactorily with analytical theories. On this basis, electron-proton temperature relaxation in our MD simulations has been correctly carried out with negligible statistical errors (Fig. 3).

[1] J. D. Lindl, P. Amendt, R. L. Berger, S. G. Glendinning, S. H. Glenzer, S. W. Haan, R. L. Kauffman, O. L. Landen, L. J. Suter, The physics basis for ignition using indirectdrive targets on the National Ignition Facility, Phys. Plasmas **11**, 339 (2004).

[2] S. Atzeni and J. Meyer-ter-Vehn, The physics of inertial fusion (Clarendon Press, Oxford, 2004).

[3] O. A. Hurricane, D. A. Callahan, D. T. Casey, P. M. Celliers, C. Cerjan, E. L. Dewald, T. R. Dittrich, T. Döppner, D. E. Hinkel, L. F. Berzak Hopkins *et al.*, Fuel gain exceeding unity in an inertially confined fusion implosion, Nature (London) **506**, 343 (2014).

[4] R. Betti, and O. A. Hurricane, Inertial-confinement fusion with lasers, Nat. Phys. **12**, 435 (2016).

[5] Z. F. Fan, J. Liu, B. Liu, C. X. Yu, and X. T. He, Ignition conditions relaxation for central hot-spot ignition with an ion-electron nonequilibrium model, Phys. Plasmas **23**, 010703 (2016).

[6] Z. F. Fan, Y. Y. Liu, B. Liu, C. X. Yu, K. Lan, and J. Liu, Non-equilibrium between ions and electrons inside hot spots from National Ignition Facility experiments, Matter Radiat. Extremes **2**, 3 (2017).

[7] A. B. Zylstra, O. A. Hurricane, D. A. Callahan, A. L. Kritcher, J. E. Ralph, H. F. Robey, J. S. Ross, C. V. Young, K. L. Baker, D. T. Casey *et al.*, Burning plasma achieved in inertial fusion, Nature (London) **601**, 542 (2022).

[8] K. Lan, Dream fusion in octahedral spherical hohlraum, Matter Radiat. Extremes **7**, 055701 (2022).

[9] B. I. Cho, T. Ogitsu, K. Engelhorn, A. A. Correa, Y. Ping, J. W. Lee, L. J. Bae, D. Prendergast, R. W. Falcone, and P. A. Heimann, Measurement of electron-ion relaxation in warm dense copper, Sci. Rep. **6**, 18843 (2016).

[10] A. Alberti, A. Munafò, M. Nishihara, C. Pantano, J. B. Freund, and M. Panesi, Non-equilibrium plasma generation via nanosecond multi-mode laser pulses, J. Appl. Phys. **131**, 033102 (2022).

[11] L. B. Fletcher, J. Vorberger, W. Schumaker, C. Ruyer, S. Goede, E. Galtier, U. Zastrau, E. P. Alves, S. D. Baalrud, R. A. Baggott *et al.*, Electron-ion temperature relaxation in warm dense hydrogen observed with picosecond resolved X-ray scattering, Front. Phys. **10**, 838524 (2022).

[12] J. Castro, P. McQuillen, H. Gao, and T. C. Killian, The role of collisions and strong coupling in ultracold plasmas, J. Phys.: Conf. Ser. **194**, 012065 (2009).

[13] S. D. Bergeson, S. D. Baalrud, C. L. Ellison, E. Grant, F. R. Graziani, T. C. Killian, M. S. Murillo, J. L. Roberts, and L. G. Stanton, Exploring the crossover between high-energy-density plasma and ultracold neutral plasma physics, Phys. Plasmas **26**, 100501 (2019).

[14] R. T. Sprenkle, L. G. Silvestri, M. S. Murillo, and S. D. Bergeson, Temperature relaxation in strongly-coupled binary ionic mixtures, Nat. Commun. **13**, 15 (2022).

[15] J. Vink, S. Broersen, A. Bykov, and S. Gabici, On the electron-ion temperature ratio established by collisionless shocks, Astron. Astrophys. **579**, A13 (2015).

[16] J. C. Raymond, P. Ghavamian, A. Bohdan, R. Dongsu, N. Jacek, S. Lorenzo, T. Aaron, A. Elena, H. Masahiro, P. Martin, A. Takanobu, and F. Federico, Electron-ion temperature ratio in astrophysical shocks, Astrophys. J. **949**, 50 (2023).

[17] L. D. Landau, Kinetic equation in the case of the Coulomb interaction, Phys. Z. Sowjetunion **10**, 154 (1936).

[18] L. Spitzer, Jr., *Physics of Fully Ionized Gases*, 2nd ed. (Interscience, New York, 1962).

[19] L. G. stanton, and M. S. Murillo, Ionic transport in high-energy-density matter, Phys. Rev. E **93**, 043203 (2016).

[20] A. Lenard, On Bogoliubov's kinetic equation for a spatially homogeneous plasma, Ann. Phys. **10**, 390 (1960).

[21] R. Balescu, Irreversible processes in ionized gases, Phys. Fluids **3**, 52 (1960).

[22] E. A. Frieman and D. L. Book, Convergent classical kinetic equation for a plasma, Phys. Fluids **6**, 1700 (1963).

[23] T. Kihara and O. Aono, Unified theory of relaxations in plasmas, I. Basic theorem, J. Phys. Soc. Jpn. **18**, 837 (1963).

[24] H. A. Gould and H. E. DeWitt, Convergent kinetic equation for a classical plasma, Phys. Rev. **155**, 68 (1967).

[25] D. Muchmore, Diffusion in white dwarf stars, Astrophys. J. **278**, 769 (1984).

[26] C. Paquette, C. Pelletier, G. Fontaine, and G. Michaud, Diffusion coefficients for stellar plasmas, Astrophys. J. Suppl. Ser. **61**, 177 (1986).

[27] D. O. Gericke, M. S. Murillo, and M. Schlanges, Dense plasma temperature equilibration in the binary collision approximation, Phys. Rev. E **65**, 036418 (2002).

[28] L. S. Brown, D. L. Preston, and R. L. Singleton Jr., Charged particle motion in a highly ionized plasma, Phys. Rep. **410**, 237 (2005).

[29] L. S. Brown and R. L. Singleton Jr., Temperature equilibration in a fully ionized plasma: Electron-ion mass ratio effects, Phys. Rev. E **79**, 066407 (2009).

[30] S. D. Baalrud, and J. Daligault, Effective potential theory for transport coefficients across coupling regimes, Phys. Rev. Lett. **110**, 235001 (2013).

[31] P. E. Grabowski, M. P. Surh, D. F. Richards, F. R. Graziani, and M. S. Murillo, Molecular dynamics simulations of classical stopping Power, Phys. Rev. Lett. **111**, 215002 (2013).

[32] S. D. Baalrud, and J. Daligault, Extending plasma transport theory to strong coupling through the concept of an effective interaction potential, Phys. Plasmas **21**, 055707 (2014).

[33] C. R. Scullard, S. Serna, L. X. Benedict, C. L. Ellison, and F. R. Graziani, Analytic expressions for electron-ion temperature equilibration rates from the Lenard-Balescu equation, Phys. Rev. E **97**, 013205 (2018).

[34] G. Dimonte and J. Daligault, Molecular-dynamics simulations of electron-ion temperature relaxation in a classical Coulomb plasma, Phys. Rev. Lett. **101**, 135001 (2008).

[35] J. N. Glosli, F. R. Graziani, R. M. More, M. S. Murillo, F. H. Streitz, M. P. Surh, L. X. Benedict, S. Hau-Riege, A. B. Langdon, and R. A. London, Molecular dynamics simulations of temperature equilibration in dense hydrogen, Phys. Rev. E **78**, 025401(R) (2008).

[36] L. X. Benedict, M. P. Surh, J. I. Castor, S. A. Khairallah, H. D. Whitley, D. F. Richards, J. N. Glosli, M. S. Murillo, C. R. Scullard, P. E. Grabowski, D. Michta, and F. R. Graziani, Molecular dynamics simulations and generalized Lenard-Balescu calculations of electron-ion temperature equilibration in plasmas, Phys. Rev. E **86**, 046406 (2012).

[37] Q. Ma, J. Y. Dai, D. D. Kang, Z. X. Zhao, J. M. Yuan, X. Q. Zhao, Molecular dynamics simulation of electron-ion temperature relaxation in dense hydrogen: A scheme of truncated Coulomb potential, High Energy Density Phys. **13**, 34 (2014).

[38] Y. Zhao, Investigation of effective impact parameters in electron-ion temperature relaxation via Particle-Particle Coulombic molecular dynamics, Phys. Lett. A **381**, 2944 (2017).

[39] C. Z. Gao, C. B. Zhang, Y. Cai, Y. Wu, Z. F. Fan, P. Wang, and J. G. Wang, Assessment of the electron-proton energy relaxation rates extracted from molecular dynamics simulations in weakly-coupled hydrogen plasmas, Phys. Rev. E **107**, 015203 (2023).

[40] F. R. Graziani, V. S. Batista, L. X. Benedict, J. I. Castor, H. Chen, S. N. Chen, C. A. Fichtl, J. N. Glosli, P. E. Grabowski, A. T. Graf *et al.*, Large-scale molecular dynamics simulations of dense plasmas: The Cimarron Project, High Energy Density Phys. **8**, 105 (2012).

[41] T. Dunn and A. A. Broyles, Method for determining the thermodynamic properties of the quantum electron gas, Phys. Rev. **157**, 156 (1967).

[42] J. P. Hansen, and I. R. McDonald, Thermal relaxation in a strongly coupled two-temperature plasma, Phys. Lett. A **97**, 42 (1983).

[43] C. Deutsch, M. M. Gombert, H. Minoo, Classical modelization of symmetry effects in the dense high-temperature electron gas, Phys. Lett. A **66**, 381 (1978); Classical modelization of symmetry effects in the dense high-temperature electron gas: Errata, **72**, 481 (1979).

[44] J. P. Hansen and I. R. McDonald, *Theory of Simple Liquids*, 3rd ed. (Academic, New York, 2006).

[45] W. H. Barkas, J. N. Dyer, and H. H. Heckman, Resolution of the Σ^--Mass Anomaly, Phys. Rev. Lett. **11**, 26 (1963).

[46] N. R. Shaffer and S. D. Baalrud, The Barkas effect in plasma transport, Phys. Plasmas **26**, 032110 (2019).

[47] H. J. C. Berendsen, J. P. M. Postma, W. F. van Gunsteren, A. DiNola, J. R. Haak, Molecular dynamics with coupling to an external bath, J. Chem. Phys. **81**, 3684 (1984).

[48] W. C. Swope, H. C. Andersen, P. H. Berens, K. R. Wilson, A computer simulation method for the calculation of equilibrium constants for the formation of physical clusters of molecules: Application to small water clusters, J. Chem. Phys. **76**, 637 (1982).

[49] P. J. Adrian, R. Florido, P. E. Grabowski, R. Mancini, B. Bachmann, L. X. Benedict, M. G. Johnson, N. Kabadi, B. Lahmann, C. K. Li *et al.*, Measurements of ion-electron energy-transfer cross section in high-energy-density plasmas, Phys. Rev. E **106**, L053201 (2022).